Crystal Structures of the Yeast Prion Ure2p Functional Region in Complex with Glutathione and Related Compounds[†,⊥]

Luc Bousset,[‡] Hassan Belrhali,[§,||] Ronald Melki,*[,‡] and Solange Morera[‡]

Laboratoire d'Enzymologie et Biochimie Structurales, CNRS, Avenue de la Terrasse, 91198 Gif-sur-Yvette, France, and European Synchrotron Radiation Facility, Boîte Postale 220, 38043 Grenoble Cedex, France

Received May 17, 2001; Revised Manuscript Received August 27, 2001

ABSTRACT: The [URE3] phenotype in yeast *Saccharomyces cerevisiae* is due to an altered prion form of Ure2p, a protein involved in nitrogen catabolism. To understand possible conformational changes at the origin of prion propagation, we previously solved the crystal structure of the Ure2p functional region [Bousset et al. (2001) *Structure 9*, 39−46]. We showed the protein to have a fold similar to that of the β class of glutathione *S*-transferases (GSTs). Here we report crystal structures of the Ure2p functional region (extending from residues 95−354) in complex with glutathione (GSH), the substrate of all GSTs, and two widely used GST inhibitors, namely, *S*-hexylglutathione and *S*-*p*-nitrobenzylglutathione. In a manner similar to what is observed in many GSTs, ligand binding is not accompanied by a significant change in the conformation of the protein. We identify one GSH and one hydrophobic electrophile binding site per monomer as observed in all other GSTs. The sulfur group of GSH, that conjugates electrophiles, is located near the amide group of Asn124, allowing a hydrogen bond to be formed. Biochemical data indicate that GSH binds to Ure2p with high affinity. Its binding affects Ure2p oligomerization but has no effect on the assembly of the protein into amyloid fibrils. Despite results indicating that Ure2p lacks GST activity, we propose that Ure2p is a member of the GST superfamily that may describe a novel GST class. Our data bring new insights into the function of the Ure2p active region.

The protein Ure2 is part of the signal transduction cascade that regulates nitrogen catabolism in the yeast *Saccharomyces cerevisiae* (*1*). When rich nitrogen sources are available, Ure2p represses the expression of several gene products involved in the use of poor nitrogen sources. The [URE3] phenotype (*2*) is due to a transmissible conformational change of Ure2p (*3*). The prion (infectious protein) form of Ure2p has lost its function and gained the capacity to transform the active form of the protein into its inactive form (*4*). It has also acquired the ability to assemble into amyloid fibrils (*4, 5*). Ure2p is composed of two distinct regions (*5, 6*). The N-terminal region (residues 1−93) is rich in asparagine and glutamine residues (43 of 93 amino acids) and is sufficient to induce [URE3] phenotype (*7, 8*). The C-terminal region (residues 94−354) is the functional part of the protein since it complements *URE2* gene deletion (*9*).

We previously solved the crystal structure of the Ure2p functional region (extending from amino acids 95 to 354) (*10*). The protein is a homodimer, and each monomer is formed by two domains (*6, 10*−*12*). The N-terminal domain (residues 95−196) is composed of a central four-stranded β-sheet flanked by four α-helices, two on both sides, while the C-terminal domain (residues 206−354) is entirely α-helical. Despite the low degree of sequence identity (less than 20%) between Ure2p and members of the GST[1] superfamily (*9*), they share similar fold and quaternary structure. These results suggest that Ure2p belongs to the GST superfamily.

GSTs are ubiquitous enzymes that protect cells against many xenobiotic substances and products of oxidative stress. They achieve this function by catalyzing the nucleophilic attack of the sulfur atom of the tripeptide glutathione (GSH, γ-Glu-Cys-Gly) on these electrophilic groups (*13*). They are assorted into nine distinct families, alpha, beta, delta, theta, mu, pi, sigma, phi, and omega, based on substrate specificity and primary structure identity (*14*). Crystal structures from each class of the GST superfamily in complex with various inhibitors and substrates have been reported (*14*−*20*). These studies have shown that the overall polypeptide fold is similar and that the active site consists of two binding pockets: the G site where GSH binds and the H site where hydrophobic

[†] This work was supported by the Centre National de la Recherche Scientifique, the Association pour la Recherche sur le Cancer, and the Actions Concertées Program of the French Ministry of Research and Technology.

[⊥] The coordinates for Ure2p crystal form I in complex with glutathione and *S*-*p*-nitrobenzylglutathione and that of crystal form II in complex with *S*-hexylglutathione, have been deposited in the Protein Data Bank with accession numbers 1jzr, 1k0b, 1k0d, 1k0c, 1k0a, respectively.

* Correspondence should be addressed to this author. Phone: 33 1 69 82 35 03, Fax: 33 1 69 82 31 29, E-mail: melki@lebs.cnrs-gif.fr.

[‡] Laboratoire d'Enzymologie et Biochimie Structurales, CNRS.

[§] European Synchrotron Radiation Facility.

[||] Present address: EMBL Grenoble Outstation, BP181, 38042 Grenoble Cedex 9, France.

[1] Abbreviations: GST, glutathione *S*-transferase; GSH, glutathione; rms, root-mean-square; HEPES, *N*-(2-hydroxyethyl)piperazine-*N*′-2-ethanesulfonic acid; ADAN-glutathione, acetyl-2-dimethylaminonaphthaleneglutathione.

10.1021/bi011007b CCC: $20.00
Published on Web 10/20/2001

electrophiles bind. The G site is formed by residues from the N-terminal domain while the H site is mainly formed by residues of the C-terminal domain (*13*). *S*-Hexyl- and *S*-*p*-nitrobenzylglutathione are inhibitors of GSTs. The hexyl- and *p*-nitrobenzyl groups bind to the H site and occupy the position of the hydrophobic electrophile substrates.

Here we present high-resolution crystal structures of Ure2p 95−354 in complex with GSH and *S*-hexyl- and *S*-*p*-nitrobenzylglutathione. We identify and delineate two binding sites located in a cleft between the N- and C-terminal domains: one glutathione and one hydrophobic electrophile binding site. They together form a typical GST active site. A comparison of the active sites of Ure2p 95−354 and various GSTs is presented. Finally, the effect of GSH on Ure2p oligomerization and assembly into amyloid fibrils is examined and discussed.

EXPERIMENTAL PROCEDURES

Purification and Crystallization. Ure2p from residues 95−354 was overexpressed in *Escherichia coli* and purified using the procedure described in Thual et al. (*12*). Native Ure2p 95−354 crystals of forms I and II were obtained using the crystallization conditions described in Bousset et al. (*10*). These crystals were soaked in 5 mM GSH, *S*-hexylglutathione, or *S*-*p*-nitrobenzylgutathione (SIGMA), from 10 min to 1 month before data collection. Cryoprotection was achieved by adding 20% glycerol, before freezing at 100 K. All crystals belong to space group $P2_12_12_1$ with various cell parameters (Table 1). Form I crystals contain two dimers per asymmetric unit while the form II asymmetric unit is solely composed of a dimer.

Data Collection. Data collection experiments were carried out at $\lambda = 0.934$ Å on ID14-EH1 beamline of the European Synchrotron Radiation Facility (Grenoble). Diffraction patterns were recorded on a 165 mm diameter MarResearch CCD detector. For each complex, a single crystal was used to collect a complete data set. Data were processed and scaled with the programs DENZO (*21*) and SCALA (*22*). The relevant data statistics are presented in Table 1.

Structure Determination and Refinement. The structure of all Ure2p complexes was determined using the native model of either form I or form II (*10*). They were refined using similar protocols. A rigid-body refinement followed by several cycles of positional refinement using CNS (*23*) and manual rebuilding was performed. The first $2F_o-F_c$ and F_o-F_c electron density maps were examined using TurboFRODO (*24*) and revealed in each case clear density for both the protein and the ligands. The ligands were built, and water molecules were gradually added during further conjugate gradient refinement with CNS. Statistics for the five refined models are given in Table 1. They have *R*-factors in the range 20−21% (R_{free} 26−27%) and very good stereochemistry.

Binding of Acetyl-2-dimethylaminonaphthaleneglutathione to Ure2p. Glutathione, 50 mM, in HEPES, pH 7.5, was incubated with 20 mM 6-bromoacetyl-2-dimethylaminonaphthalene (Molecular Probes, Inc., Eugene, OR) for 2 h at room temperature in order to allow the formation of a thioether bond between the SH group of the molecule and the probe. Binding of acetyl-2-dimethylaminonaphthaleneglutathione (ADAN-glutathione) to full-length Ure2p and Ure2p 95−354 in 50 mM Tris, pH 7.5, 100 mM KCl was monitored in a 10 × 2 mm quartz cuvette (Hellma) thermostated at 20 °C in an AMINCO−Bowman series 2 spectrofluorometer. The excitation and emission monochromators were set at 380 and 500 nm, respectively.

Table 1: Crystallographic Data and Refinement Statistics

	GSH	GSH	GSH	*S*-*p*-nitrobenzyl	*S*-hexyl
			Data		
space group	$P2_12_12_1$	$P2_12_12_1$	$P2_12_12_1$	$P2_12_12_1$	$P2_12_12_1$
cell parameters					
a (Å)	54.6	54.5	54.7	54.7	54.5
b (Å)	124.9	124.9	122.3	123.2	77.2
c (Å)	161.2	160.8	166.9	168.2	126.2
$\alpha = \beta = \gamma$ (deg)	90	90	90	90	90
resolution (Å)	2.9	2.5	2.2	2.5	2.5
measured intensities	369804	353357	381950	390942	144989
unique reflections	25150	38915	57630	38381	18419
completeness (%)	99.5	99.9	99.3	94.0	96.9
I/σ	3.2	6.7	7.8	7.4	9.0
R_{sym} (%)[a]	10.4	10.6	7.1	8.0	6.6
			Refinement		
resolution range (Å)	20−2.9	20−2.5	20−2.2	20−2.5	20−2.5
reflections	24911	38605	56901	37263	18180
protein atoms	8057	7956	7593	7628	3722
solvent molecules	0	210	291	161	71
ligand atoms	40	40	60	110	46
R_{cryst} (%)[b]	20.9	20.6	21.3	21.4	21.8
R_{free} (%)[c]	27.6	26.4	26.2	26.7	26.7
			RMS Deviation		
bond length (Å)	0.008	0.007	0.006	0.007	0.007
bond angles (deg)	1.33	1.25	1.16	1.23	1.23
average *B* (Å^2)					
protein					
Mol A	15.43	27.40	33.43	35.91	47.16
Mol B	18.01	32.74	35.00	32.22	47.30
Mol C	13.64	27.07	32.81	33.69	
Mol D	13.67	26.12	35.34	36.16	
ligand					
Mol A	19.21	51.74	45.63	54.94	57.53
Mol B			48.94	68.38	59.25
Mol C	16.70	50.81	38.00	41.34	
Mol D				54.63	

[a] $R_{sym} = \Sigma|I_i - \langle I\rangle|/\Sigma I_i$, where I_i is the intensity of a reflection and $\langle I\rangle$ is the average intensity of that reflection. [b] $R_{cryst} = \Sigma||F_{obs}| - |F_{calc}||/\Sigma|F_{obs}|$. [c] 5% of the data were set aside for R_{free} calculation.

Competition experiments were performed by two means. Labeled ADAN-glutathione was added to increasing amounts of GSH and the mixture used in the binding assay. Alternatively, increasing amounts of unlabeled GSH were added to full-length Ure2p or Ure2p 95−354 saturated by ADAN-glutathione, and the decrease in fluorescence was monitored. The two methods gave similar results, indicating that GSH binds to Ure2p in an exchangeable manner.

Assembly of Ure2p into Amyloid Fibrils. Assembly of Ure2p into amyloid fibrils was monitored using a thioflavin-T binding assay (*25*). Ure2p solution (60 μM) was incubated at 4 °C. At regular time intervals, 8 μL aliquots were removed from the solution, mixed with 300 μL of thioflavin-T (Sigma), and incubated at 20 °C for 10 min. Thioflavin-T binding was measured by averaging the emission signal over 30 s using an AMINCO−Bowman series 2 spectrofluorometer set at 440 nm (excitation) and 480 nm (emission). Ure2p fibrils assembled in the absence or the presence of GSH (2 mM) in 20 mM Tris, pH 7.5, 100 mM KCl were negatively stained on carbon-coated grids (200 mesh) with 1% uranyl acetate and examined in a Philips EM 410 electron miscroscope.

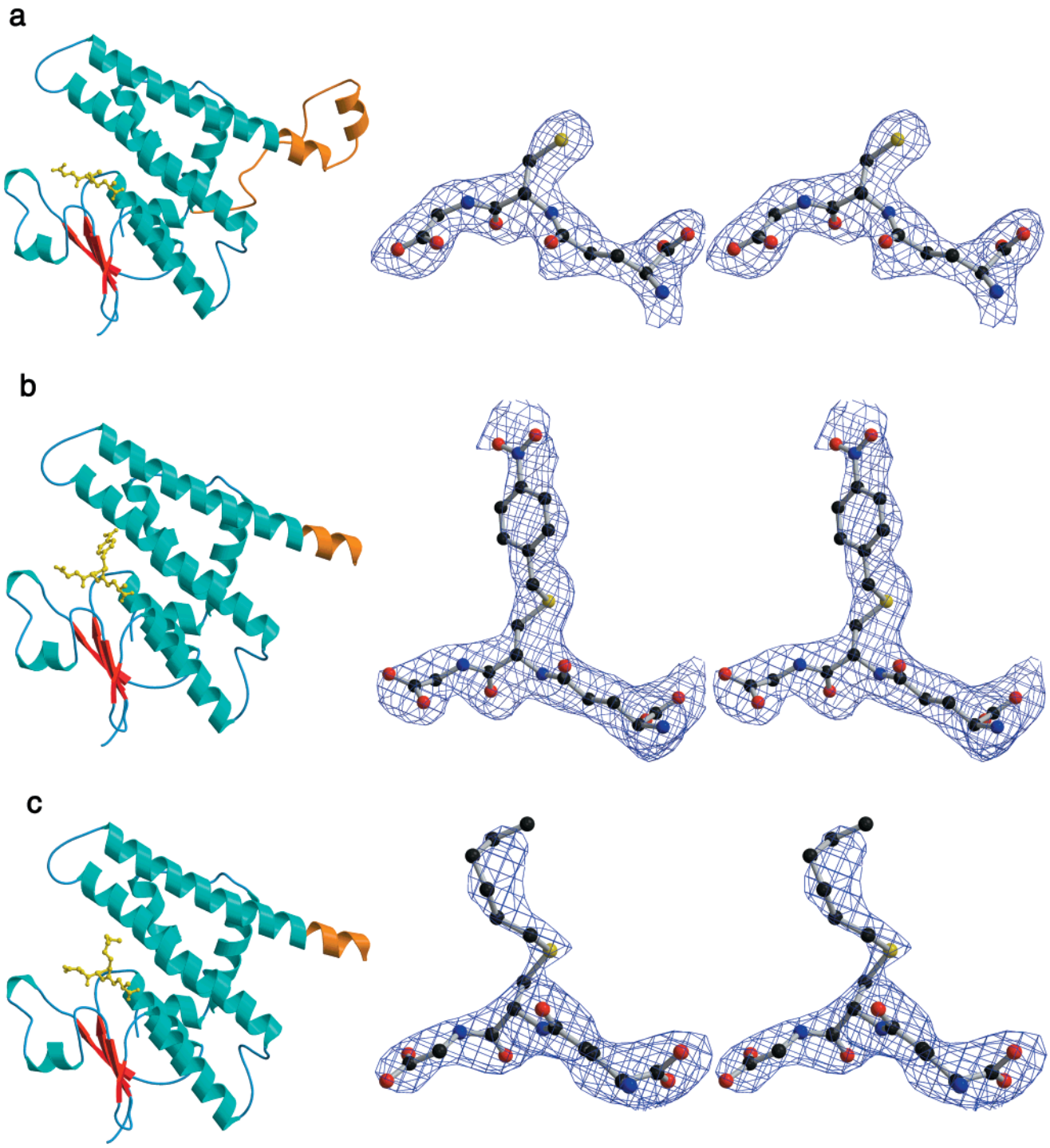

FIGURE 1: Ribbon representation of Ure2p 95−354 monomer in complex with (a) glutathione, (b) *S*-*p*-nitrobenzylglutathione, and (c) *S*-hexylglutathione. The *β*-sheet in the small N-terminal domain is in red, and α-helices are in blue. The cap region (residues 267−298) is in orange. All ligands are drawn as yellow balls and sticks, and are shown in the F_o-F_c electron density omit map contoured at 2 sigma (stereoview). Drawn with Molscript (*42*), Bobscript (*43*), and Raster3D (*44*).

Sedimentation Velocity Measurements. Sedimentation velocity experiments were carried out as described (*5*). Measurements were made at 40 000 rpm and 18 °C. Data were analyzed to provide the apparent distributions of sedimentation coefficients using the programs SVEDBERG (*26*) and DC/DT (*27*).

RESULTS

Ure2p 95−354−GSH Complexes. We previously solved two crystal forms (forms I and II) of the Ure2p functional region (*10*). Form I asymmetric unit is composed of two dimers, one formed by monomers A and B and the other by monomers C and D. Form II asymmetric unit is solely composed of a dimer (molecules A and B). The structure of Ure2p 95−354 in complex with GSH was solved in crystal form I at 2.9, 2.5, and 2.2 Å resolution. A glutathione is bound to monomers A and C in the three complexes and to monomer B in the 2.2 Å resolution complex. The cap region (residues 267−298) (*10*) is disordered in all dimers AB and only in dimer CD at 2.2 Å resolution. There are no

observable differences between these three complexes. The average rms deviation is 0.37 Å for all Cα positions excluding the cap region, and GSH binds at the same position in the cleft between the N- and C-terminal domains. GSH is well-defined in its F_o-F_c electron density omit map (Figure 1a). We will focus on dimer CD at 2.9 Å resolution given that the mean temperature factor is the lowest (Table 1). The fold of monomer C with a bound GSH is shown in Figure 1a. The structures of unliganded Ure2p 95−354 and in complex with GSH are highly similar, the average rms deviation being 0.3 Å for Cα positions in dimer CD.

Ure2p 95−354−S-p-Nitrobenzylglutathione and −S-Hexylglutathione Complexes. The cap region of form I *S-p*-nitrobenzylglutathione complex is disordered in dimers AB and CD. The *S-p*-nitrobenzylglutathione binds to each monomer. However, as the electron density of the *p*-nitrobenzyl group is poorly defined in molecule D, a GSH has been modeled. The structure of the *S*-hexylglutathione complex was determined in form II (*10*). Here also, the cap region is badly defined in both monomers. Both monomers interact with an *S*-hexylglutathione. However, as the *S*-hexyl moiety is disordered in molecule B, only the GSH part of the ligand was kept. The *S-p*-nitrobenzylglutathione and *S*-hexylglutathione complexes are presented in Figure 1b,c, respectively, and the ligands in their respective F_o-F_c electron density omit maps are shown. Ligand binding has no effect on the overall protein structure. The superposition of all Cα positions (excluding the cap region) of the unliganded and *S-p*-nitrobenzylglutathione structures gives a rms deviation of 0.45 Å. A similar superposition with the *S*-hexylglutathione complex gives a rms deviation of 0.53 Å due to a local change affecting an external loop (residues 150−155). When these residues are omitted, the rms deviation is 0.44 Å, indicating that the rest of the structure is unaffected by the presence of the GST inhibitor.

The G and H Binding Sites. The binding sites of glutathione and the hydrophobic electrophiles are called G and H, respectively. In all complexes described in this work, glutathione is bound at the same position and in the same conformation. It is located in the cleft between the N- and C-terminal domains at the top of the β-sheet (Figure 1). GSH binds close to the β1-to-α2 loop, the α3-to-β3 loop, and the N-terminus of helix α4 with its γ-glutamyl moiety pointing toward the core of Ure2p 95−354 and its glycyl moiety pointing toward helix α3. It interacts solely with the N-terminal domain of the protein (Figure 2a). The distances are listed in Table 2. Glu180 that adopts unusual main-chain dihedral angles is hydrogen-bonded to the nitrogen atom of the γ-glutamyl group. Both hydroxyl and amino groups of Ser181 make polar contacts with the carboxylate oxygens of the γ-glutamyl moiety. The carbonyl and amino groups of Val165 interact in an antiparallel β-sheet manner with the main-chain atoms of the GSH Cys residue. The Arg164 and His151 side chains are hydrogen-bonded to the carboxylate group of the glycyl moiety. Ala122, Pro123, and the phenyl group of Phe146 make van der Waals contacts with GSH. The sulfur group, that conjugates electrophiles, is located near the amide group of Asn124, allowing a hydrogen bond to be formed (Table 2). The *p*-nitrobenzyl and hexyl moieties occupy the same position in a hydrophobic pocket formed by the side chain atoms of Ser121, Pro123, Leu231, Trp316, Val319, and Arg322 (Figure 2b,c).

Table 2: Contacts between Ure2p 95−354 and Ligands[a]

ligand	ligand atom	protein atom	Mol A (Å)	Mol B (Å)	Mol C (Å)
GSH	N1 (γ-Glu)	OE1 Glu180	3.25		3.25
		OE2 Glu180	2.66		3.25
	O11 (γ-Glu)	OG Ser181	3.17		2.83
	O12 (γ-Glu)	N Ser181	2.92		2.88
	N2 (Cys)	O Val165	2.84		2.65
	O2 (Cys)	N Val165	3.05		2.83
	SG2 (Cys)	ND2 Asn124	3.16		3.48
	O31 (Gly)	NE2 His151	3.04		3.15
	O32 (Gly)	NE Arg164	3.30		3.13
S-nitrobenzyl	C2	O Ser121	3.51	3.68	
	C3	O Ser121	3.03	3.15	3.21
	C4	O Ser121	3.41	3.49	
	C5	CD1 Leu231	3.64	3.62	3.56
		CZ3 Trp316	3.76		3.64
	C6	CD Pro123	3.57	3.61	
		CH2 Trp316	3.57		3.55
		CZ3 Trp316	3.47		3.45
	N4	CD1 Leu231	3.70		3.52
		NH2 Arg322	3.41	3.13	
	O1N	CD1 Leu231	3.33		2.94
		CG1 Val319	3.22	3.14	
		CG2 Val319	3.43		3.70
		NH2 Arg322	3.39	2.69	
	O2N	NH2 Arg322	2.98	2.80	2.78
	SG2 (Cys)	ND2 Asn124	3.41	3.86	3.57
S-hexyl	C1	CH2 Trp316	3.73		
		ND2 Asn124	3.94		
	C4	CD1 Leu231	3.65		
	C5	CD1 Leu231	3.68		
		O Ser121	3.80		
	C6	CD Pro123	3.53		
		CG Pro123	3.62		
		CD1 Leu231	3.66		
		CZ3 Trp316	3.73		
	SG2 (Cys)	ND2 Asn124	3.90		

[a] Polar and van der Waals contacts are less than 3.5 and 4 Å, respectively.

The C-terminal domain through residues from helices α5 and α7 and two residues of the β1-α2 loop in the N-terminal part contribute to the large H site. In the *p*-nitrobenzylglutathione complex, the guanidinium of Arg322 interacts with the nitroxide group (Table 2). The Arg322 side chain adopts a different position in the hexyl complex.

Binding of GSH, *S*-hexylglutathione, and *S-p*-nitrobenzylglutathione buries 627, 780, and 866 Å^2 of accessible surface area within each monomer, respectively. The solvent-accessible surface areas were calculated using the program ASA (Prof. A. Lesk, Cambridge; probe size 1.4 Å).

Comparison of the G and H Sites between Ure2p and GSTs. The fold and ligand sites of Ure2p 95−354 resemble those of the β class GSTs (Figure 3a). GSH binds at the same place and in the same orientation (Figure 3b). The structure-based sequence alignment (*10*) between Ure2p 95−354 and *E. coli* (*17*) and *Proteus mirabilis* (*18*) bacterial GSTs is shown in Figure 4. In the GST superfamily, each subunit has an active site composed of a G and an H site located in equivalent positions. Ure2p possesses the same cleft and the two binding sites. In addition, its backbone conformation and its interaction mode with GSH are similar to those of all GST classes. The common constituents of the G site are conserved in Ure2p 95−354 (Figures 2 and 4). They involve the following: (i) the paired hydrogen bonds in an antiparallel arrangement between the cysteinyl back-

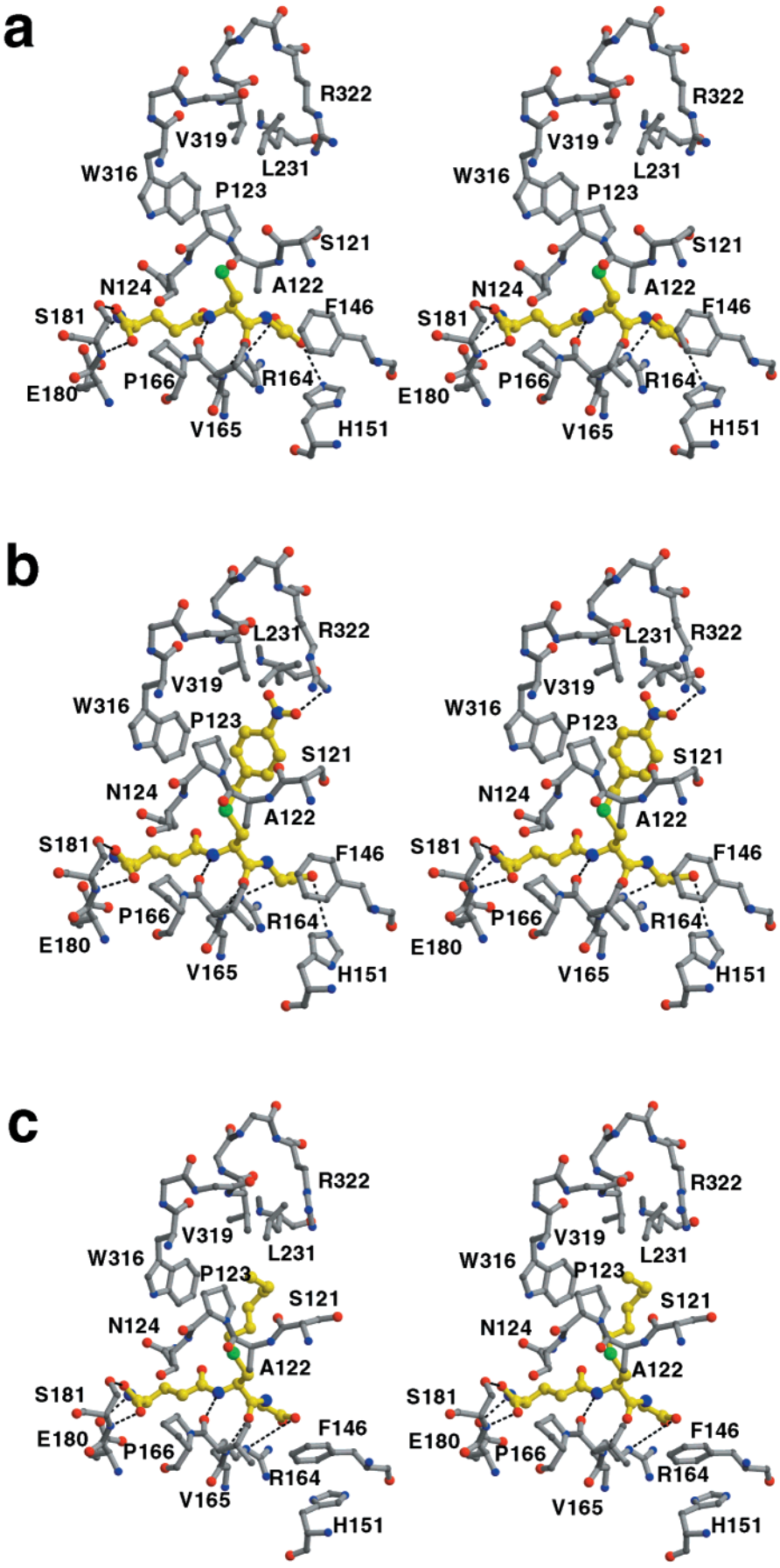

FIGURE 2: Ball and stick stereoview of the G and H sites in the three Ure2p 95−354 complexes. The ligands are in yellow, and residues are labeled. Dotted lines indicate hydrogen bonds. (a) Glutathione complex, (b) *S*-*p*-nitrobenzylglutathione complex, and (c) *S*-hexylglutathione complex.

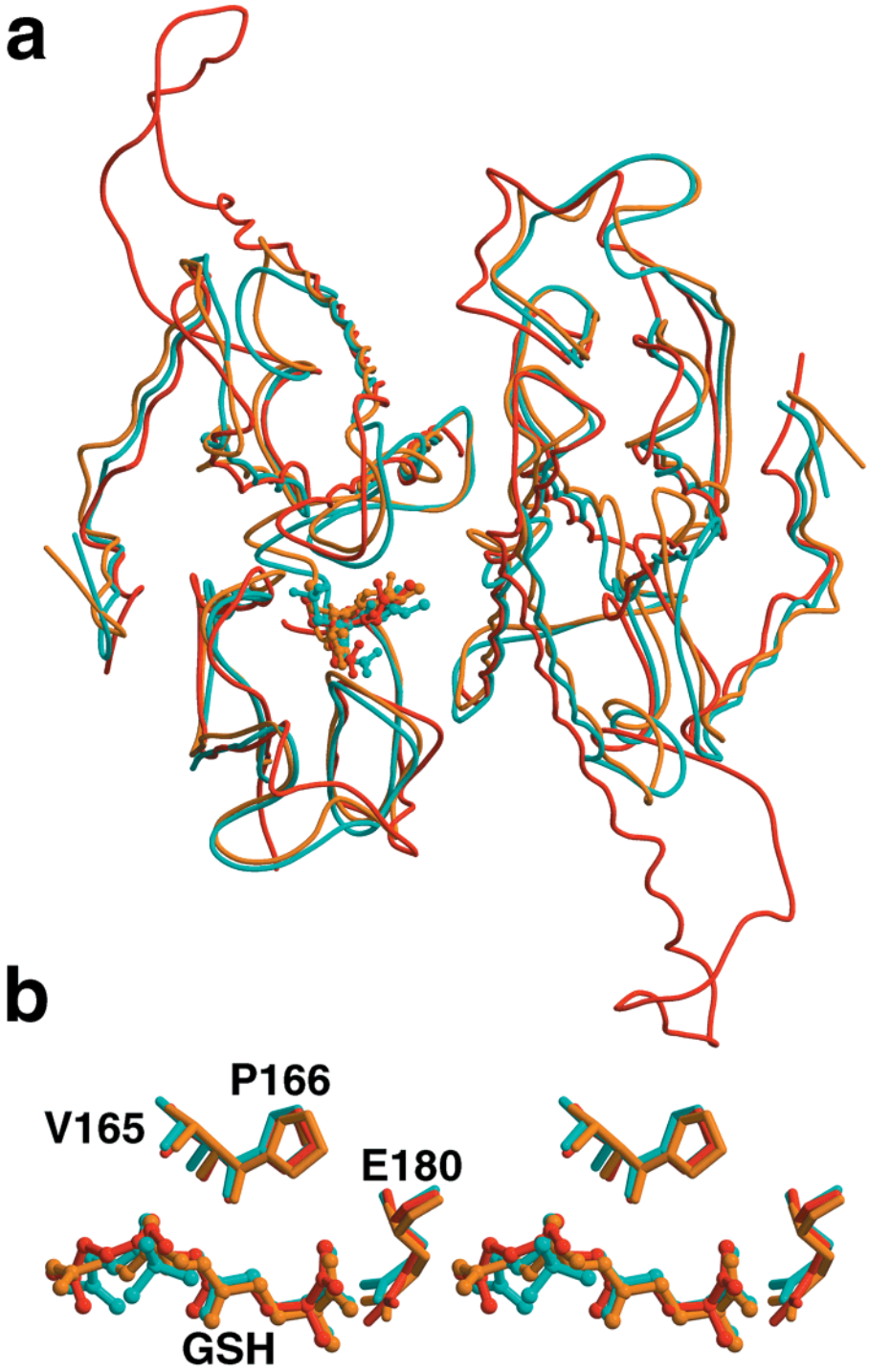

FIGURE 3: Superposition of Ure2p 95−354 and *E. coli* and *P. mirabilis* GST dimers in complex with GSH. (a) Ure2p 95−354 is in red, *E. coli* GST in cyan, and *P. mirabilis* GST in orange. (b) Stereo closeup view of the GSH binding site in the three superimposed structures. The three strictly conserved residues involved in GSH binding are labeled.

bone atoms of GSH and Val165 (Val52 of beta GSTs); (ii) the cis conformation of Pro166 (Pro53 of beta GSTs); and (iii) Glu180 with its unusual main-chain dihedral angles (Glu65 of beta GSTs). The side chain of Arg164 in Ure2p makes van der Waals contacts and is hydrogen-bonded to the backbone atoms of GSH. In bacterial and eukaryotic GSTs, a Gln or an Asn side chain (Gln51 in beta GSTs) located at an equivalent position in space forms a similar contact. Ser181 in Ure2p [Gly66 in beta GSTs; Ser63, -65, or -67 in eukaryotic GSTs (*28*)] makes identical contacts with the γ-glutamyl group of GSH. Most of the residues involved in GSH binding or in the architecture of the active site belong to the α3-to-β3 loop (residues 160−168) which is highly conserved between bacterial GSTs and Ure2p (Figure 4). Among the 15 strictly conserved residues between the N-terminal domain of Ure2p 95−354 and bacterial GSTs, 2 residues (Val165 and Glu180 in Ure2p) bind GSH and 6 contribute to the architecture of the active site (Asn160, Pro161, cis-Pro166, Leu168, Ala183, and Ile184; Figure 4). The major difference between the active sites of Ure2p and bacterial GSTs is due to the nature of the residue that interacts with the thiol group of GSH. Indeed, in bacterial

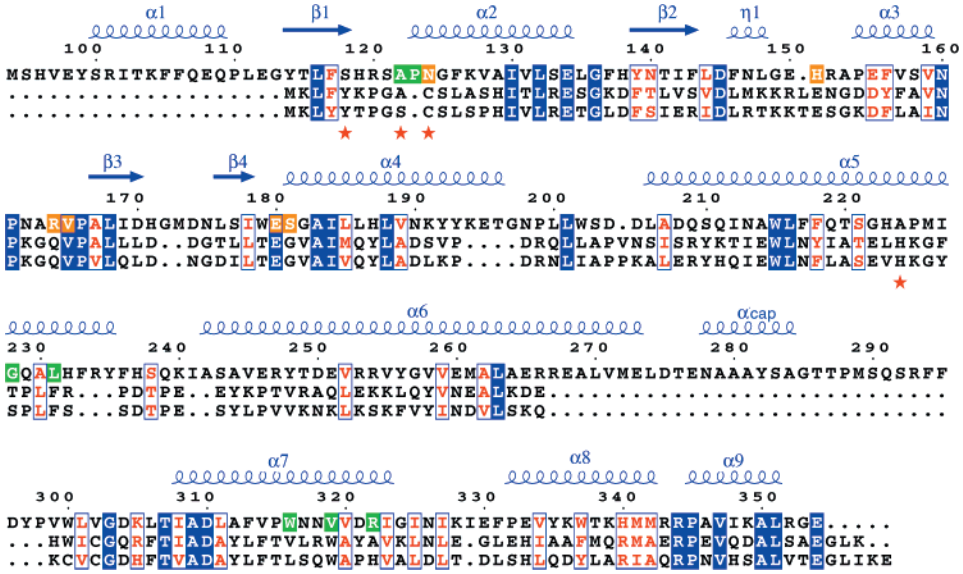

FIGURE 4: Structure-based sequence alignment of Ure2p 95−354 and two bacterial GSTs. The two bacterial GSTs are *E. coli* GST (accession code 1aof) and *P. mirabilis* GST (accession code 2pmt). The secondary structure elements of Ure2p 95−354 are labeled and indicated by coils for α-helices, arrows for β-sheets, and η for 3_{10} turns. Homologous residues are in red while identical residues are shown as white letters on a blue background. Residues belonging to the G (GSH binding site) and H (hydrophobic electrophile binding site) sites that interact with glutathione and its analogues are shown as white letters on an orange and a green background, respectively. The positions of the catalytic tyrosine or serine of the eukaryotic classes of GSTs (*13*, *15*, *16*, *45*−*47*) and the catalytic cysteine and histidine of the β class GSTs (*17*, *18*) are indicated by red stars. The figure was created using ESPript (*48*).

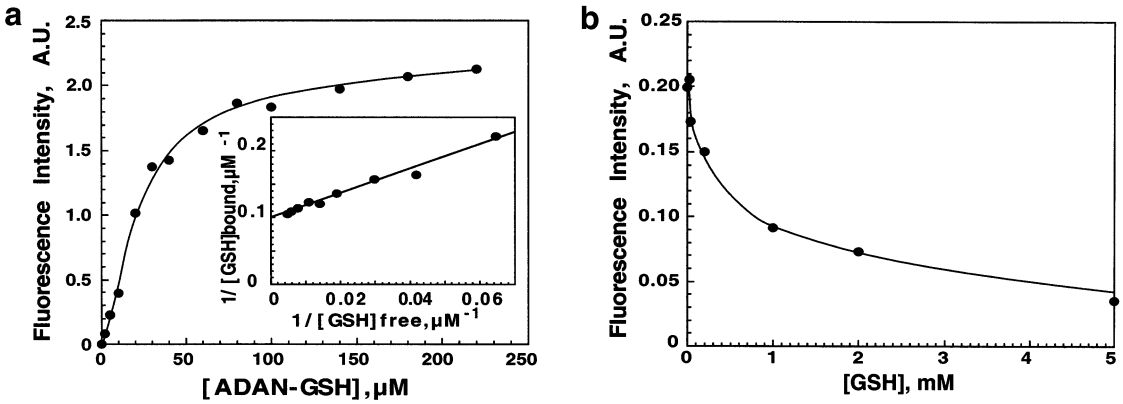

FIGURE 5: Binding of ADAN-glutathione to Ure2p. (a) Amount of bound ADAN-glutathione to Ure2p. The solid curve is the calculated isotherm for binding of ADAN-glutathione to a single category of sites (10 μM) and an equilibrium dissociation constant of 20 μM. Inset: double-reciprocal plot of the data. (b) Competition between unlabeled glutathione and ADAN-glutathione for binding to Ure2p. ADAN-glutathione (20 μM) bound to Ure2p (3.8 μM) was chased by increasing concentrations of unlabeled glutathione in 50 mM Tris, pH 7.5, 100 mM KCl.

GSTs, Cys10 interacts with the sulfur atom of GSH, while in Ure2p, the equivalent residue, Asn124, is at the right distance to form a hydrogen bond with the thiol group (Table 2). Ure2p and bacterial GSTs differ by an additional amino acid (Pro123 in Ure2p). A similar additional amino acid is also present in all the other GST classes (*18*).

In contrast to the highly conserved G site in the GST superfamily, the H site is variable. This is likely due to the large variety of electrophilic substrates. The H sites of Ure2p and bacterial GSTs are wider and more polar than those of most other GSTs (*18*). Its architecture is similar in Ure2p and bacterial GSTs despite a difference in the amino acid sequence (Figure 4). However, the location and packing of the residues create different pocket shapes in the two proteins.

Binding of Glutathione to Ure2p. Binding of glutathione to Ure2p is not accompanied by a change in the intrinsic fluorescence of the protein. We therefore labeled the thiol group of glutathione with extrinsic environment-sensitive fluorophores. The acetyl-2-dimethylaminonaphthaleneglutathione derivative (ADAN-glutathione) showed a significant increase in fluorescence upon binding to Ure2p. ADAN-glutathione binds to Ure2p with a stoichiometry of 1:1, and an apparent equilibrium dissociation constant of 20 μM in 20 mM Tris, pH 7.5 at 20 °C (Figure 5a). Unmodified glutathione inhibited the binding of labeled glutathione competitively with an equilibrium constant of 22 μM (Figure 5b).

Effect of Glutathione on Ure2p Oligomerization and Assembly into Amyloid Fibrils. We previously showed that the major oligomeric species of full-length Ure2p and Ure2p 95−354 in solution is a dimer (*5*, *12*). We also brought evidence for a concentration-dependent tetramerization of full-length Ure2p. To determine whether glutathione binding influences the oligomeric state of the protein, we carried out sedimentation velocity experiments in the presence and the

Table 3: Relative Abundance of the Oligomeric Species of Full-Length Ure2p and Ure2p 95−354 in the Absence or the Presence of GSH[a]

	$s^0_{20,w}$ (S)				
	3.9	4.3	5.6	6.5	11
Ure2p		93		5	0
Ure2p + GSH		42		32	23
Ure2p 95−354	95		4		
Ure2p 95−354 + GSH	48		51		

[a] Sedimentation velocity experiments were performed in the absence or the presence of GSH (1 mM) at 18 °C and 60 000 rpm. Full-length Ure2p (0.8 mg/mL) and Ure2p 95−354 (1.5 mg/mL) are in 50 mM Tris, pH 7.5, 100 mM KCl.

absence of glutathione and analyzed them to yield the apparent distribution of sedimentation coefficients, $g^*(s)$. The data are summarized in Table 3. Whereas the sedimentation coefficients of the oligomeric species of full-length Ure2p (0.8 mg/mL) are unaffected by binding of GSH, their proportions vary significantly upon GSH binding. The proportion of the dimeric species decreases from 93 to 42%; that of the tetrameric species increases from 5 to 32%. In addition, a species accounting for 23% of the material with a sedimentation coefficient of 11 S, compatible with the molecular mass of a Ure2p octamer, forms. Binding of GSH to Ure2p 95−354 (1.5 mg/mL) also results in a decrease of the proportion of dimeric species from 95 to 48% and an increase in the proportion of tetrameric species from 4 to 51%. We conclude from these experiments that binding of GSH to Ure2p affects its oligomeric state and favors higher molecular weight species.

The effect of GSH on the assembly of Ure2p into amyloid fibrils was monitored using thioflavin-T binding. The assembly kinetics of Ure2p into amyloid fibrils in the absence and the presence of GSH are similar (Figure 6a). In addition, the fibrils appear identical in shape and length when examined in the electron microscope (Figure 6b,c). We conclude from these experiments that GSH has no effect on the assembly of Ure2p into amyloid fibrils.

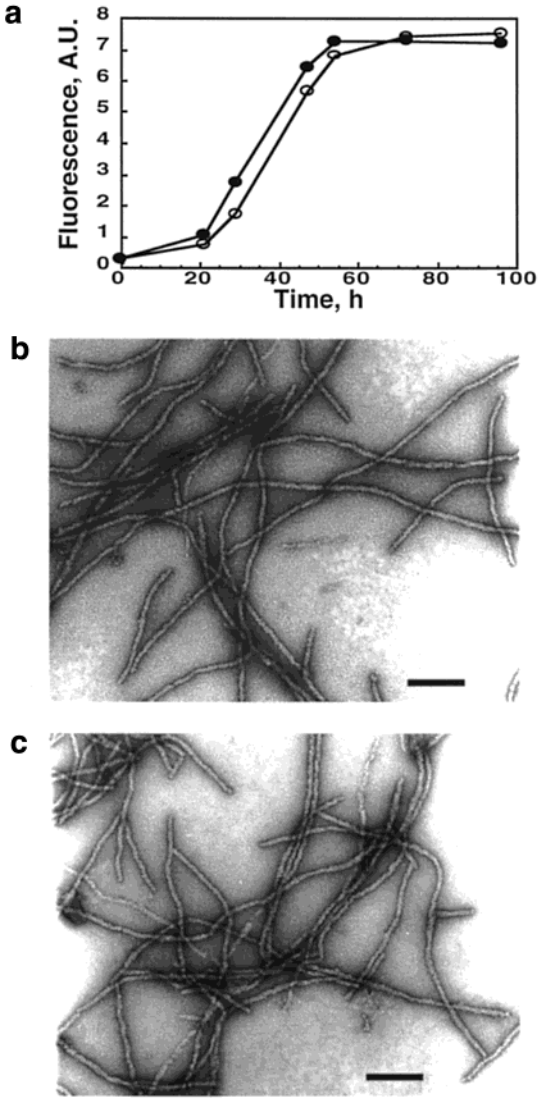

FIGURE 6: Ure2p assembly into amyloid fibrils is unaffected by GSH. (a) Time course of Ure2p (60 μM) assembly into amyloid fibrils in 50 mM Tris, pH 7.5, 100 mM KCl, in the absence (○) or the presence (●) of GSH (1 mM), was monitored by Thioflavin-T binding. Electron micrographs of negatively stained Ure2p fibrils assembled in the absence (b) or the presence (c) of GSH (2 mM). Bar = 0.2 μm.

DISCUSSION

We previously demonstrated that the Ure2p functional region has a fold similar to that of GSTs, in particular the β class of GSTs (*10*). We identified a cleft running along the domain interface that resembles the active site of all GSTs. We hypothesized that it could be a potential ligand binding site and suggested that Ure2p belongs to the GST superfamily.

In this study, we demonstrate that Ure2p binds GSH with high affinity. It also binds GSH-related compounds, *S*-*p*-nitrobenzyl- and *S*-hexylglutathione, in a manner similar to other GSTs. We show that Ure2p possesses G and H binding pockets that can form an active site. Thus, we propose that Ure2p is a GST for which the specific substrate is yet unidentified.

None of the proposed catalytic residues among GST classes is present in Ure2p (*10*) (Figure 4). The only polar group near the thiol group of GSH is the amide group of Asn124. The absence of a detectable activity using a standard GST test, i.e., 1-chloro-2,4-dinitrobenzene as substrate (*6*, *9*, *29*), means neither that Ure2p is a member of the GST superfamily nor that it is inactive. Indeed, a number of eukaryotic GSTs perform specific functions (*30*−*32*) while bacterial GSTs catalyze reactions that are specific to prokaryotes and exhibit either minimal or no detectable activity toward a range of standard GST substrates (*33*−*37*).

The activity of Ure2p may be regulated by two features, the Asn- and Gln-rich N-terminal region and its flexible α-cap. The N-terminal region modulates the capacity of the protein to assemble and may regulate its enzymatic activity or turnover alone or together with the flexible α-cap as revealed in the Ure2p double mutant S10L/V271E where prion-induction increases 10-fold (*38*). These two regions may also play specific roles in the interaction with partner proteins (*9*, *39*, *40*).

The mechanism by which Ure2p regulates nitrogen catabolism is not yet understood. The binding of ligands to Ure2p could modulate its affinity toward partner proteins. Alternatively, Ure2p could act on a protein that regulates

nitrogen catabolism by mediating its posttranslational modification or catalyzes the condensation to GSH of a low molecular weight substrate, yielding a product that binds and modulates the activity of a protein involved in the regulation of nitrogen catabolism.

Binding of GSH does not induce conformational changes on Ure2p nor does it affect its assembly into amyloid fibrils. This clearly indicates that filling the G pocket is not sufficient to induce a conformational change at sites involved in fibril assembly. Such changes could nevertheless occur upon binding of the yet unidentified substrate of Ure2p to its H pocket. Thus, GSH is not by itself an allosteric regulator of Ure2p assembly. Interestingly, however, binding of GSH affects the Ure2p oligomeric state. It decreases the proportion of dimers and increases that of tetramers, octamers, and higher molecular weight species. Similar oligomers, frequently observed in electron micrographs, coexist with amyloid fibrils (*5*). The kinetics of Ure2p assembly into fibrils would be affected by the presence of GSH if these oligomers were the precursors of amyloid fibrils and their formation the rate-limiting step in the reaction. This is not what is observed here. Thus, either the high molecular weight oligomers are not the precursors of amyloid fibrils or their formation is not rate-limiting. It is very likely that Ure2p fibrils form by the association of the high molecular weight oligomers we observe since the assembled form of Ure2p binds GSH with high affinity (Bousset et al., in preparation). This finding suggests that the conformation of Ure2p 95−354 is not altered in the fibrils, in agreement with the absence of significant differences in the proteolytic patterns of soluble and assembled Ure2p (*5*). In addition, Ure2p high molecular weight oligomers form rapidly and are in equilibrium with the dimeric form of the protein (L. Bousset and R. Melki, unpublished data). Thus, one could speculate that the rate-limiting step in the assembly of Ure2p oligomers into fibrils is their association and subsequent lock into these filamentous structures in a manner similar to what has been observed for the Sup35 protein (*41*).

The finding that Ure2p possesses typical G and H sites suggests that it is an active GST. The absence of detectable enzymatic activity is likely due to the use of improper substrates. Thus, special efforts should be done to identify Ure2p substrate(s). In addition, extensive site-directed mutagenesis of the Ure2p cleft together with the identification of the physical partners of Ure2p should allow a better understanding of the role of this binding site and its possible role in nitrogen regulation and prion formation.

ACKNOWLEDGMENT

We thank the staff of ESRF in Grenoble for making station ID14-EH1 available. We thank Joël Janin for his support and very helpful discussions.

REFERENCES

1. Magasanik, B. (1992) in *The Molecular and Cellular Biology of the Yeast Saccharomyces cerevisiae* (Jones, E. W., Pringle, J. R., and Broach, J. R., Eds.) Vol. 2, pp 283−317, Cold Spring Harbor Laboratory Press, Plainview, NY.
2. Aigle, M., and Lacroute, F. (1975) *Mol. Gen. Genet. 136*, 327−335.
3. Wickner, R. B. (1994) *Science 264*, 566−569.
4. Taylor, K. L., Cheng, N., Williams, R. W., Steven, A. C., and Wickner, R. B. (1999) *Science 283*, 1339−1343.
5. Thual, C., Komar, A. A., Bousset, L., Fernandez-Bellot, E., Cullin, C., and Melki, R. (1999) *J. Biol. Chem. 274*, 13666−13674.
6. Perret, S., Freeman, S. J., Butler, J. G., and Fersht, A. R. (1999) *J. Mol. Biol. 290*, 331−345.
7. Masison, D. C., and Wickner, R. B. (1995) *Science 270*, 93−95.
8. Masison, D. C., Maddelein, M. L., and Wickner, R. B. (1997) *Proc. Natl. Acad. Sci. U.S.A. 94*, 12503−12508.
9. Coschigano, P. W., and Magasanik, B. (1991) *Mol. Cell. Biol. 11*, 822−832.
10. Bousset, L., Belrhali, H., Janin, J., Melki, R., and Morera, S. (2001) *Structure 9*, 39−46.
11. Umland, T., Taylor, K. L., Rhee, S., Wickner, R. B., and Davies, D. R. (2001) *Proc. Natl. Acad. Sci. U.S.A. 98*, 1459−1464.
12. Thual, C., Bousset, L., Komar, A. A., Walter, S., Buchner, J., Cullin, C., and Melki, R. (2001) *Biochemistry 40*, 1764−1773.
13. Wilce M. C. J., and Parker M. W. (1994) *Biochim. Biophys. Acta 1205*, 1−18.
14. Board, P. G., Coggan, M., Chelvanayagam, G., Easteal, S., Jermiin, L. S., Schulte, G. K., Danley, D. E., Hoth, L. R., Griffor, M. C., Kamath, A. V., Rosner, M. H., Chrunyk, B. A., Perregaux, D. E., Gabel, C. A., Geoghegan, K. F., and Pandit, J. (2000) *J. Biol. Chem. 275*, 24798−24806.
15. Dirr, H. W., Reinemer, P., and Hubert, R. (1994) *Eur. J. Biochem. 220*, 645−661.
16. Armstrong, R. N. (1997) *Chem. Res. Toxicol. 10*, 2−18.
17. Nishida, M., Harada, S., Nogushi, S., Satow, Y., Inoue, H., and Takahashi, K. (1998) *J. Mol. Biol. 281*, 135−147.
18. Rossjohn, J., Polekhina, G., Feil, S. C., Allocati, N., Masulli, M., De Illio, C., and Parker, M. W. (1998) *Structure 6*, 721−734.
19. Oakley, A. J., Lo Bello, M., Battistoni, A., Ricci, G., Rossjohn, J., Villar, H. O., and Parker, M. W. (1997) *J. Mol. Biol. 274*, 84−100.
20. Garcia-Saez, I., Parraga, A., Phillips, M. F., Mantle, T. J., and Coll, M. (1994) *J. Mol. Biol. 237*, 298−314.
21. Otwinowski, Z., and Minor, W. (1997) *Methods Enzymol. 276*, 307−326.
22. CCP4 (Collaborative Computational Project 4) (1994) *Acta Crystallogr., Sect. D D50*, 760−763.
23. Brunger, A. T., Adams, P. D., Clore, G. M., DeLano, W. L., Gros, P., Grosse-Kunstleve, R. W., Jiang, J. S., Kuszewski, J., Nilges, M., Pannu, N. S., Read, R. J., Rice, L. M., Simonson, T., and Warren, G. L. (1998) *Acta Crystallogr., Sect. D D54*, 905−921.
24. Roussel, A., and Cambillau, C. (1989) Turbo-FRODO. in *Silicon graphics Geometry Partners Directory* (Silicon Graphics, Ed.) pp 77−78, Silicon Graphics, Mountain View, CA.
25. McParland, V. J., Kad, N. M., Kalverda, A. P., Brown, A., Kirwin-Jones, P., Hunter, M. G., Sunde, M., and Radford, S. E. (2000) *Biochemistry 39*, 8735−8746.
26. Philo, J. S. (1994) Measuring sedimentation, diffusion, and molecular weights of small molecules by direct fitting of sedimentation velocity concentration profiles. in *Modern Analytical Ultracentrifugation* (Schuster, T. M., and Laue, T. M., Eds.) pp 156−170, Birkhäuser, Boston.
27. Stafford, W. F., III (1992) *Anal. Biochem. 203*, 295−301.
28. Reinemer, P., Prade, L., Hof, P., Neuefeind, T., Huber, R., Zettl, R., Palme, K., Schell, J., Koelln, I., Bartunik, H. D., and Bieseler (1996) *J. Mol. Biol. 255*, 289−309.
29. Choi, J. H., Lou, W., and Vancura, A. (1998) *J. Biol. Chem. 273*, 29915−29922.
30. Tomarev, S. I., and Zinovieva, R. D. (1988) *Nature 336*, 86−88.
31. Bruns, C. M., Hubatsch, I., Ridderström, M., Mannervik, B., and Tainer, J. A. (1999) *J. Mol. Biol. 288*, 447−439.
32. Ji, X., von Rosenvinge, E. C., Johnson, W. W., Tomarev, S. I., Piatigorsky, J., Armstrong, R. N., and Gilliland, G. L. (1995) *Biochemistry 34*, 5317−5328.

33. Di llio, C., Aceto, A., Piccolomini, R., Allocati, N., Faraone, A., Cellini, L., Ravagnan, G., and Federici, G. (1988) *Biochem. J. 255*, 971−975.
34. Iizuka, M., Inoue, Y., Murata, K., and Kimura, A. (1989) *J. Bacteriol. 171*, 6039−6042.
35. La Roche, S. D., and Leisinger, T. (1990) *J. Bacteriol. 172*, 164−171.
36. Nishida, M., Kong, K.-H., Inoue, H., and Takahashi, K. (1994) *J. Biol. Chem. 269*, 32536−32541.
37. Vuilleumier, S. (1997) *J. Bacteriol. 179*, 1431−1441.
38. Fernandez-Bellot, E., Guillemet, E., and Cullin, C. (2000) *EMBO J. 19*, 3215−3222.
39. Edskes, H. K., Hanover, J. A., and Wickner, R. B. (1999) *Genetics 153*, 585−594.
40. Hardwick, J. S., Kuruvilla, F. G., Tong, J. K., Shamji, A. F., and Schreiber, S. L. (1999) *Proc. Natl. Acad. Sci. U.S.A. 96*, 14866−14870.
41. Serio, T. R., Cashikar, A. G., Kowal, A. S., Sawicki, G. J., Moslehi, J. J., Serpell, L., Arnsdorf, M. F., and Lindquist, S. L. (2000) *Science 289*, 1317−1321.
42. Kraulis, P. J. (1991) *J. Appl. Crystallogr. 24*, 946−950.
43. Esnouf, R. M. (1997) *J. Mol. Graphics 15*, 132−134.
44. Merritt, E. A., and Bacon, D. J. (1997) *Methods Enzymol. 277*, 505−524.
45. Wilce, M. C. J., Board, P. G., Feil, S. C., and Parker, M. W. (1995) *EMBO J. 14*, 2133−2143.
46. Board, P. G., Coggan, M., Wilce, M. C. J., and Parker, M. W. (1995) *Biochem. J. 311*, 247−250.
47. Tan, K.-L., Chelvanayagam, G., Parker, M. W., and Board, P. G. (1996) *Biochem. J. 319*, 315−321.
48. Gouet, P., Courcelle, E., Stuart, D. I., and Metoz, F. (1999) *Bioinformatics 15*, 305−308.

BI011007B